Atmos. Chem. Phys. Discuss., 14, 707–750, 2014
www.atmos-chem-phys-discuss.net/14/707/2014/
doi:10.5194/acpd-14-707-2014

Atmospheric Chemistry and Physics
Open Access
Discussions

New-particle formation, growth and climate-relevant particle production in Egbert, Canada: analysis from one year of size-distribution observations

J. R. Pierce[1,2], **D. M. Westervelt**[3], **S. A. Atwood**[1], **E. A. Barnes**[1], **and W. R. Leaitch**[4]

[1]Department of Atmospheric Science, Colorado State University, Fort Collins, CO, USA
[2]Department of Physics and Atmospheric Science, Dalhousie University, Halifax, NS, Canada
[3]Program in Science, Technology, and Environmental Policy (STEP), Princeton University, Princeton, NJ, USA
[4]Environment Canada, Toronto, Ontario, Canada

Received: 2 December 2013 – Accepted: 23 December 2013 – Published: 10 January 2014

Correspondence to: J. R. Pierce (jeffrey.pierce@colostate.edu)

Published by Copernicus Publications on behalf of the European Geosciences Union.

ACPD
14, 707–750, 2014

New-particle formation, growth and climate-relevant particle production

J. R. Pierce et al.

Abstract

Aerosol particle nucleation, or new-particle formation, is the dominant contributor to particle number in the atmosphere. However, these particles must grow through condensation of low-volatility vapors without coagulating with the larger, pre-existing particles in order to reach climate-relevant sizes (diameters larger than 50–100 nm), where the particles may affect clouds and radiation. In this paper, we use one year of size-distribution measurements from Egbert, Ontario, Canada to calculate the frequency of regional-scale new-particle formation events, new-particle formation rates, growth rates and the fraction of new particles that survive to reach climate-relevant sizes. Regional-scale new-particle formation events occurred on 14–31 % of the days (depending on the stringency of the classification criteria), with event frequency peaking in the spring and fall. New-particle formation rates and growth rates were similar to those measured at other mid-latitude continental sites. We calculate that roughly half of the climate-relevant particles (with diameters larger than 50–100 nm) at Egbert are formed through new-particle formation events. With the addition of meteorological and SO_2 measurements, we find that new-particle formation often occurred under synoptic conditions associated with high surface pressure and large-scale subsidence that cause sunny conditions and clean-air flow from the north and west. However, new-particle formation also occurred when air flow came from the polluted regions to the south and southwest of Egbert. The nucleation rates tend to be faster during events under the polluted south/southwest flow conditions.

1 Introduction

Atmospheric aerosols may impact climate directly by scattering and absorbing solar radiation, and indirectly by modifying the albedo and lifetime of clouds (Forster et al., 2007). For both of these effects, aerosols with diameters larger than 50–100 nm dominate the climate effects since (1) accumulation-mode (∼ 100–1000 nm particles) tend

ACPD
14, 707–750, 2014

to dominate the direct scattering/absorption effects in most parts of the atmosphere (Charlson et al., 1992; Seinfeld and Pandis, 2006) and (2) particles larger than about 50–100 nm act as Cloud Condensation Nuclei (CCN), the seeds upon which cloud droplets form (e.g. Dusek et al. (2006); Seinfeld and Pandis, 2006). (The actual lower cutoff diameter for CCN depends on the updraft velocity in the cloud and the composition of the aerosols.)

Aerosol nucleation, the formation of new ~ 1 nm particles by the aggregation of low-volatility vapor molecules (including sulfuric acid, organics, ammonia and water), is likely the largest contributor to aerosol number in the atmosphere (Kulmala et al., 2004; Pierce and Adams, 2009; Spracklen et al., 2006). When nucleated particles grow to sizes where they are measured in the atmosphere (between 1–10 nm depending on the measurement instruments), the phenomena is generally called new-particle formation to distinguish these measured events from nucleation, which may be occurring even when not measured by some instruments. New-particle formation has been observed in a large number of continental boundary-layer (BL) locations, the free troposphere and some marine locations (e.g. Kulmala et al. (2004) and references therein).

While new-particle formation occurs in many regions of the atmosphere and contributes a significant number of particles, these new particles must grow to larger sizes (50–100 nm) in order to have an appreciable affect on climate. The growth of the new particles occurs primarily through the condensation of sulfuric acid vapor and low-volatility organic vapors (Boy et al., 2005; Kuang et al., 2012; Kulmala et al., 2005; Riipinen et al., 2011, 2012). However, these growing particles may be removed, primarily by coagulation with larger particles, before reaching climate-relevant sizes. The competition between condensational growth and coagulational losses has led to the adoption of the term Survival Probability (SP) for the fraction of newly formed particles that grows to a climate-relevant size without being scavenged through coagulation (Kuang et al., 2009; Pierce and Adams, 2007; Westervelt et al., 2013). In environments with a large source of condensible vapors and a low amount of pre-existing particles, new particles grow quickly (both due to the high production of condensible

ACPD
14, 707–750, 2014

vapors and the low sink of condensible vapors to the pre-existing particles) and are lost by coagulation slowly. Under these conditions, the survival probability is high and has been observed to exceed 99 % (to 50 nm) in some atmospheric conditions (Westervelt et al., 2013). On the other hand, under conditions with a small source of condensible vapors and a high amount of pre-existing particles, the survival probability is low and has been observed to be less than 1 % under these conditions (Westervelt et al., 2013). In order to understand how nucleation and new-particle formation contributes to climate-relevant aerosol concentrations, both new-particle formation rates and survival probabilities must be understood in different atmospheric regions and under varying conditions.

New-particle formation may occur over relatively small spatial scales (kilometers or smaller) in plumes from individual sources or clumps of sources (e.g. an urban plume) (Junkermann et al., 2011; Lonsdale et al., 2012; Stevens and Pierce, 2013; Stevens et al., 2012; Yu, 2010), or it may occur more homogeneously over relatively large spatial scales (100s of kilometers) when a synoptic air mass is relatively homogeneous for both aerosols/gases and meteorology (Jeong et al., 2010). For regional-scale nucleation, new-particle formation and growth rates may be calculated from the timeseries of aerosol size-distribution measurements at stationary sites (Dal Maso et al., 2005). This is done by observing how the number of particles at the smallest observed sizes changes with time and by observing the growth in the diameter of these particles. These properties can be calculated only when the air mass is homogeneous. In air masses that have aerosol size distributions that vary spatially, aerosol size distributions will change due to advection. If the air mass is assumed to be constant in cases where it is not, there may be apparent appearances, disappearances, growth or shrinking of particles that are not due to physical new-particle formation and growth. In these inhomogeneous cases, particles formed via new-particle formation are still observed by stationary measurement sites, but the air-mass properties change too quickly to determine the formation and growth rates.

ACPD
14, 707–750, 2014

Recent studies have used observations of regional nucleation and growth to determine the survival probability of particles at various measurement sites (Kuang et al., 2009; Westervelt et al., 2013). These studies showed that if the air mass over a measurement site is homogeneous for long enough, the growth of new particles to climate-relevant sizes may be explicitly tracked. These direct observations of new-particle formation rates, growth rates and new-particle survival probability are essential for testing the ability of aerosol microphysics models to correctly predict the sources of CCN and other climate-relevant particles in the atmosphere. Westervelt et al. (2013) used the observed values from five locations to test multiple nucleation schemes in the GEOS-Chem-TOMAS global chemical transport model with online aerosol microphysics, and the model generally reproduces nucleation and growth frequency and rates at these locations. Additionally, Kerminen et al. (2012) calculated the contribution of new-particle formation to CCN concentrations at four locations by looking at the change in CCN concentrations before and after the growing nucleation mode reached a CCN size threshold. Thus, they were able to calculate the CCN contribution without using growth rates and survival probabilities.

Given that these recent studies have quantified the contribution of regional nucleation events to the production of climate-relevant particles in several locations, it is useful to understand the factors that contribute to the occurrence of regional nucleation events in order to further test model predictions. Previous studies have shown that more intense solar radiation (which can enhance photochemistry), high concentrations of precursor species of low-volatility condensible material (e.g. SO_2 and biogenic volatile organic compounds), and low concentrations of pre-existing aerosols (i.e. a low condensation and coagulation sink) all create favorable conditions for regional new-particle formation and growth (Donahue et al., 2011; Kulmala et al., 2005; Pierce et al., 2011, 2012; Sihto et al., 2006). Thus, measurement sites that can provide statistics on nucleation rates, growth rates, survival probabilities along with information on the factors that contribute to nucleation/growth events will provide a basis for testing fundamental physical and chemical processes in aerosol models.

ACPD
14, 707–750, 2014

In this study, we use one year of size-distribution measurements (May 2007–May 2008) to determine statistics on regional nucleation, growth and survival probability to climate-relevant sizes at Egbert, Ontario, Canada. Additionally, we look at the environmental factors that control the occurrence of these events at this location. Egbert generally experiences remote continental air when air masses move from the north and generally more polluted when air masses move from the south (Rupakheti et al., 2005); thus, like many mid-latitude continental locations, Egbert experiences a mixture of natural and anthropogenic influences (Slowik et al., 2010). Nucleation at Egbert was explored for a 3 week period with 4 other Ontario sites (Jeong et al., 2010), and nucleation at Egbert for the full year tested here was investigated for coherence with nucleation with a site in Indiana, US (Crippa and Pryor, 2013), but neither of these studies presented comprehensive statistics on nucleation, growth and the contribution to climate-relevant particles.

In the following section, we describe the methods for our analysis. In Sect. 3, we present our results, including the statistics of nucleation, growth and survival probability at Egbert as well as an analysis of the meteorological and chemical factors associated with the nucleation and growth events. The conclusions are in Sect. 4.

2 Methods

2.1 Location

The measurements used in this paper were taken from 3 May 2007 until 15 May 2008 at the Center for Atmospheric Research Experiments (CARE) in Egbert, Ontario, Canada (44.23° N, 79.78° W; 251 m a.s.l.) operated by Environment Canada. During the 2007–2008 period above, additional aerosol and gas measurements were taken, and these will be described in the following subsection. Egbert is located ~ 70 mi north of Toronto. While the region close to Egbert is a mixture of forests and farmland, Toronto and the southern Ontario region has ~ 8 million people. Thus, when winds are from the south, Egbert is influenced by the outflow from the densely populated southern Ontario region as well as the US northeast. When winds are from the north, the air generally has little recent anthropogenic influence (an exception is industry in the isolated city of Sudbury ~ 300 km to the north) and may have significant biogenic influence during the spring, summer and early fall (Slowik et al., 2010).

2.2 Instrumentation

The base meteorological measurements at the Egbert site included pressure, temperature, relative humidity, wind speed and direction (using a R. M. Young Model 05103 Wind Monitor) and solar irradiance. During the period studied in this paper, the ambient aerosol number size distribution was measured with a Scanning Mobility Particle Sizer (SMPS) system comprised of a TSI 3071 Electrostatic Classifier and a TSI 3010 Condensation Particle Counter (UCPC), which measured the size distribution from 10–420 nm with a time resolution of about 5 min. Flows were calibrated with Gilibrator and sizing was checked several times during the year with nearly monodisperse particles generated from a separate Electrostatic Classifier as well as with particles of polystyrene latex. Additional details of the SMPS system are discussed in Riipinen et al. (2011). SO_2 measurements were made with a TECO 43-S Sulfur Dioxide Monitor. Calibrations were done using a NIST traceable SO_2 gas source and a dilution system. The detection limit was 200 pptv for 15 min averages that we use here.

2.3 New-particle formation, growth and survival probability analysis

2.3.1 Event classification

We classify new-particle formation events each day using the event classification routine of Dal Maso et al. (2005), and a brief description of this classification follows. A total number of 327 days were analyzed, which is fewer than the total number of days (370) because we did not consider days that did not have SMPS measurements for at least

Discussion Paper | Discussion Paper | Discussion Paper | Discussion Paper |

ACPD
14, 707–750, 2014

New-particle formation, growth and climate-relevant particle production

J. R. Pierce et al.

75 % of the days duration (the sample time resolution is ∼ 5 min). Each analyzed day is classified as either a new-particle-formation event day or a non-event day. To be considered a new-particle-formation event day a distinct mode of particles with diameters smaller than 20 nm must appear during the day (regardless of the time at which it appears). This classification (and the event classification described below) was done visually and subjectively as done in Dal Maso et al. (2005).

For days that are considered new-particle formation days, we classify events as class 1a, class 1b and class 2 event days, also following Dal Maso et al. (2005) with the exception that our class 2 events encompass both the class 2 events and the "undefined" events in Dal Maso et al. (2005) as there was a strong continuum between these two event types in the Egbert data (most of the focus of this paper will be on the class 1a and 1b events that may be regional events). Examples of each class are given in Fig. 1; however, even within event classes, there is significant variability between event days in terms of observed behavior.

Class 1a days (e.g. Fig. 1a) exhibit new-particle formation and an obvious, traceable growth of the nucleation mode to at least 50 nm before the nucleation mode disappears. Class 1a days are most likely widespread, regional new-particle formation events with a homogeneous air mass advecting over the Egbert measurement site.

Class 1b days (e.g. Fig. 1b) exhibit new-particle formation and some growth (in some cases to over 50 nm); however, we do not trust the nucleation, growth and survival probability statistics on class 1b days to the same degree as class 1a events due to a variety of factors, which include possible changes in the air mass during the growth, shrinking after the growth (which may be a sign of a plume event), or it not being clear if the growing particles are the same particles as the newly formed particles (as is the case in Fig. 1b). Class 1b events may be regional in nature, but the air mass was not homogeneous enough to clearly track nucleation and growth from the stationary Egbert site.

Class 2 events (e.g. Fig. 2) exhibit particles being measured at the smallest sizes of the SMPS, and there is either no growth or there is growth followed by shrinking (as is

ACPD
14, 707–750, 2014

the case in Fig. 1c). These events may be particles that nucleated across spatial scales smaller than regional-scale events, such as point-source or urban plumes. They may also be small primary particles from nearby sources. In cases where particles appear to grow and then shrink, these may indicate plume nucleation events where the direction of the wind changes with time such that the smallest particles are observed when the edges of the plume are over the measurement site and the larger new particles are observed when the center of the plume is over the measurement site. Larger new particles (particles that nucleated closer to the source and have had more time to grow) are observed in the middle of plumes with more-recently nucleated particles towards the edges (Stevens et al., 2012).

2.3.2 New-particle formation and growth rates

The details of the calculation of new-particle formation and growth rates are discussed in detail in Westervelt et al. (2013), but we will briefly summarize here. The rate of new-10 nm-particle formation (J10) is calculated from the time-dependent change in the nucleation-mode (defined here as 10–25 nm) concentrations from the SMPS. We correct these formation rates for the coagulational loss rate of these particles and the loss of particles by condensational growth to sizes larger than 25 nm. The correction for these coagulational and condensational losses increases our calculated J10 from the uncorrected values. We implicitly assume that all particles entering the 10–25 nm size range are from new-particle formation during class 1a and 1b events and not from primary emissions. In this paper, we present J10 values as both the mean J10 during the period where new-particle formation was occurring (typically 2–4 h) as well as 24 h mean values to normalize the total particle production between short and long events.

The particle diameter growth rates (GR) are calculated by tracking the change in the diameter of the peak value of the aerosol size distribution for the growing nucleation mode between 10 and 25 nm. We use a linear fit of the peak diameter over time to estimate the mean growth rate during the observable growth period. When able, we also calculate the mean growth rate between 25 and 50 nm and between 25 and 100 nm us-

ACPD
14, 707–750, 2014

ing the same technique. Each of these growth rates is used for calculating the survival probability to 50 and 100 nm (described next). Growth-rate statistics are presented for the 10–25 nm size range.

2.3.3 Survival probability and climate-relevant particle formation rates

We calculate the survival probabilities to 50 and 100 nm (SP50 and SP100, respectively) by using the Probability of Ultrafine Growth (PUG) model (Pierce and Adams, 2007). These 50 and 100 nm cutoffs are used as proxies for CCN cutoffs; however, CCN cutoffs also vary as a result of aerosol composition (e.g. Paramonov et al., 2013). The application of the PUG model to SMPS measurements is described in detail in Westervelt et al. (2013). The PUG model calculates the SPs using the mean GRs described above and the coagulation sink of the growing particles to larger, pre-existing particles. The coagulation sink represents the first-order loss rate of the growing particles by coagulation, and we calculate it using the measured SMPS size distributions and Brownian coagulation theory (Seinfeld and Pandis, 2006). The PUG model calculates the survival probability over small, incremental steps of growth ($\sim$ 2 nm for 10 nm particles and $\sim$ 10 nm for 100 nm particles; these are the bin spacings of the SMPS) by calculating how many particles will be lost by coagulation in the time it takes the particles to grow by the incremental amount. For each growth step, the coagulation sink is recalculated. The overall survival probabilities to 50 or 100 nm are calculated as the products of the probabilities of surviving each incremental step.

We calculate the formation rates of climate-relevant particles (J50 and J100) as the product of the J10 with SP50 (for J50) and J10 with SP100 (for J100). We present J50 and J100 as 24 h-mean values rather than the event-mean values to represent the mean climate-relevant particle production rates on event days. These values are used to estimate the total contribution of regional-scale new-particle formation events to 50 and 100 nm particle concentrations.

ACPD
14, 707–750, 2014

2.4 Reanalysis meteorology and back trajectories

For investigating the large-scale meteorology on event days, we use the NCEP/NCAR Reanalysis (Kalnay et al., 1996). We use the 500 hPa geopotential heights, surface pressures and large-scale vertical velocities (omega) in the archives that are closest to the time of the new-particle formation events.

In order to assess the meteorological conditions and source regions associated with air masses arriving at Egbert, we utilize back trajectory analysis. The NOAA HYSPLIT Lagrangian trajectory model (Draxler, 1999; Draxler and Hess, 1997, 1998) is run using the GDAS $1^{\circ} \times 1^{\circ}$ meteorological dataset supplied by the NOAA Air Resources Laboratory. Back trajectories are shown for 24 h prior to their arrival at 100 m above ground level at Egbert. We generate eight trajectories per day with the trajectory arriving closest to the period of interest (e.g. the middle of a new-particle formation event) selected as characteristic of surface level transport at that time. We examined additional arrival heights, but these were found to be similar to the 100 m heights for trajectories arriving within the boundary layer (0 m, 500 m) and not characteristic of transport to the surface for arrival heights above the typical boundary layer (1500 m).

3 Results

Figure 2 shows the fraction of days in each month that exhibited class 1a, 1b, 2 events and non-events. Each month had at least 22 days with sufficient SMPS data to be used in the analysis (10 months had at least 26). The potentially regional new-particle formation classes, 1a (observable and quantifiable growth of new particles) and 1b (similar to 1a but less confidence in quantification), show a bimodal seasonal cycle with peaks in the spring and the fall. Either 1a or 1b events occurred on about half of the days during the peak seasons and only about 20 % of the days during summer and winter (except January where there was only one 1b event and no 1a events). Most of the 1a + 1b seasonality is driven by the seasonality of the 1a events. The winter

ACPD
14, 707–750, 2014

minimum in 1a and 1b event frequency may be due to a low source of biological volatile organic compounds (BVOCs), precursors for secondary organic aerosols that may be involved in new-particle formation and growth (Riipinen et al., 2011, 2012) as well as lower solar radiation, during cold months. Unfortunately, we do not have measurements of BVOCs or aerosol organics throughout this full time period. The summer minimum may be due to the minimum monthly mean SO_2 mixing ratios occurring during July and August. Monthly mean SO_2 mixing ratios were 0.6–0.7 ppbv during these summer months and 1–2 ppbv during the other months. Additionally, a proxy we use for H_2SO_4 concentrations (described in Sect. 3.2) also has a minimum during the summer. We go into more detail regarding these factors and the occurrence of new-particle formation events in Sect. 3.2.

Class 2 events (no quantifiable growth after new-particle detection), which may be plume-scale formation events or plumes of ultrafine primary emissions, tended to be most frequent during the winter. Up to 80 % of the days during the winter and ~ 35 % of days during the summer were class 2 days. As some class 2 events occur on days where class 1a and 1b events occurred (but these events are ignored here), this season cycle may not be this strong because there may be class 2 events hidden in class 1a and 1b event days. Regardless, the number of non-event days were highest during the summer (nearly 40 % of days during July), which may be related to the low SO_2 mixing ratios and H_2SO_4 proxy during the summer as mentioned earlier.

3.1 Particle formation rates, growth rates and CCN formation

Figure 3 shows cumulative distribution functions for J10, GR, SP50, SP100, J50 and J100 for the full year of measurements. The medians and means for these distributions as well as the total number of days in each event class are shown in Table 1. J10 and GR statistics are presented for class 1a days as well as the sum of class 1a and 1b days (we have less confidence in the statistics due to the class 1b days). We present survival probability, J50 and J100 statistics only for class 1a days as most class 1b days did not have measured growth to at least 50 nm. For J10, we present both the new-particle

ACPD
14, 707–750, 2014

formation rate averaged over the period where new-particle formation was observed (usually 2–4 h) as well as the 24 h average rate over the day (which leads to values generally 5–10 × lower than the values during the event period). J50 and J100 values are the 24 h average values. The 24 h average values are useful in that the total daily and annual production rates may be calculated from these values without needing to know the duration of each event.

The event-mean J10 values on class 1a days ranged from under 0.1 cm^{-3} s^{-1} to about 10 cm^{-3} s^{-1} with a mean of 0.84 cm^{-3} s^{-1} and median of 0.64 cm^{-3} s^{-1}. These values are about 25–50 % lower when class 1b days are also included, due to class 1b days having somewhat lower particle formation rates in general. As stated above, the 24-mean J10 values are 5–10 × lower than the event-mean values. For 1a days the 24 h mean and median values were 0.13 and 0.12 cm^{-3} s^{-1}, respectively. Westervelt et al. (2013) presented 24 h-mean new-particle formation rate statistics at 3 nm (J3) for 5 locations (Pittsburgh, Hyytiälä, Atlanta, St. Louis and the Po Valley). The observed means for the 24 h J3s at these locations ranged from 0.58 to 8.7 cm^{-3} s^{-1}, and the medians ranged from 0.09 to 0.55 cm^{-3} s^{-1}. These J3 values are generally larger than the J10 values derived here for Egbert; however, J10 values include the loss of particles by coagulation as the particles grow between 3 and 10 nm, which cause J10 values to be lower than J3.

Diameter GRs ranged from less than 0.5 to about 10 nm h^{-1} and were similar on class 1a and 1b days. The mean GR was 3.1 nm h^{-1} and the median was 2.2 nm h^{-1}. This mean and median are at the low end of the range as those analyzed by Westervelt et al. (2013) at the 5 locations. At these locations, GRs means ranged from 2.8 to 6.9 nm h^{-1} and medians ranged from 2.4 to 5.8 nm h^{-1}. The SP50 values at Egbert ranged from 1 % to close to 100 % depending on the event. This range along with the median and medians also are consistent with the 5 locations analyzed in Westervelt et al. (2013). However, the SP100 values at Egbert, which ranged from 0.3 % to over 90 % with a mean and median of 19 % and 7 % (the mean is higher than the median due to 2 high outliers, see Fig. 3) were higher than the 5 sites in Westervelt et al. (2013)

ACPD
14, 707–750, 2014

(means and medians all between 1.7 % and 4.4 %). Part of this higher SP100 in this study may be due to having a starting diameter of 10 nm in this study vs. 3 nm in Westervelt et al. (2013); however, if this were the case, we would also expect to see higher survival probabilities of growth to 50 nm in this study (compared to Westervelt et al., 2013). Additionally, in this study we follow the growing nucleation mode beyond midnight when calculating the survival probabilities, whereas in Westervelt et al. (2013) if the nucleation mode did not make it to 50 or 100 nm by midnight, it was not included in the SP analysis. It is not obvious if/how this procedural difference would bias the results. Finally, it is possible that the SP100 at Egbert was actually higher than at the 5 sites examined in Westervelt et al. (2013).

J50 is calculated as the product of J10 and SP50 for each class 1a event. The J50 values ranged from 0.001 to about 0.2 $cm^{-3} s^{-1}$, averaged over the full 24 h of each 1a-event day. The mean and median values were 0.039 and 0.029 $cm^{-3} s^{-1}$, respectively, and were within the range found at the 5 sites in Westervelt et al. (2013). Similarly, J100 is calculated as the product of J10 and SP100 for each class 1a event. The J100 values ranged from 0.001 to about 0.2 $cm^{-3} s^{-1}$, averaged over the full 24 h of each 1a-event day. The mean and median values were 0.022 and 0.009 $cm^{-3} s^{-1}$, respectively. These values were larger than 4 of the 5 sites in Westervelt et al. (2013) (the polluted Po Valley, Italy site is the exception) due to the larger SP100 values at Egbert. The median formation rates correspond to about 2500 new N50 cm^{-3} and 790 new N100 cm^{-3} on each event day. Compared to the four sites examined in Kerminen et al. (2012), our Egbert climate-relevant particle formation amounts are similar to the the amounts at Botsalano, South Africa site but are larger than the rates at the three other sites, which are located in northern Europe. However, Kerminen et al. (2012) uses a different technique for calculating the contribution of new-particle formation to climate-relevant sizes and this may lead to some differences.

We can use the J50 and J100 values to estimate the contribution of regional new-particle formation events to the number of climate-relevant particles in the region near

ACPD
14, 707–750, 2014

Egbert. The formula that we use is as follows.

$$\overline{\mathrm{N50_{NPF}}} = \frac{\overline{\mathrm{J50}} \cdot f_{1a} \cdot \mathrm{L50}}{\mathrm{BL_{rise}}} \quad (1)$$

Where $\mathrm{N50_{NPF}}$ is the annual-mean concentration of particles larger than 50 nm due to regional-scale NPF at Egbert, J50 is the mean formation rate of 50 nm particles on class 1a event days ($0.039\,\mathrm{cm^{-3}\,s^{-1}}$), f_{1a} is the fraction of analyzed days that are class 1a event day (44/327 = 0.135), L50 is the lifetime of particles larger than 50 nm in the boundary layer near Egbert, and $\mathrm{BL_{rise}}$ is the ratio of the boundary layer height when the nucleation mode reaches 50 nm to that when it reached 10 nm. Croft et al. (2013) shows that the lifetime of CCN-sized particles in the boundary layer in the mid-latitudes is around 2–4 days, so we will use a value of 3 days. Aircraft measurements of boundary-layer properties near Egbert show that the BLH increases from late morning (when the nucleation mode generally reaches 10 nm) to mid afternoon (when the nucleation mode generally reaches 50 nm) by about a factor of 2, so we will use a $\mathrm{BL_{rise}}$ value 2. With these assumptions, we calculate a $\mathrm{N50_{NPF}}$ of $682\,\mathrm{cm^{-3}}$. The mean measured N50 throughout the entire time period was $1686\,\mathrm{cm^{-3}}$. This means that about 40 % of the N50 in the region around Egbert are formed from regional-scale boundary-layer new-particle-formation events. However, there are uncertainties in L50 and $\mathrm{BL_{rise}}$. Thus, the 40 % contribution calculated here could easily be 20 % or 60 % within the range of uncertainties of these assumptions. Regardless, it is clear the new-particle formation contributes to a significant portion of the climate-relevant particles near Egbert.

We repeat the calculation to estimate $\mathrm{N100_{NPF}}$ from J100. If we assume that L100 is the same as L50 and that $\mathrm{BL_{rise}}$ is the same as the previous calculation, $\mathrm{N100_{NPF}}$ is $395\,\mathrm{cm^{-3}}$. The mean measured N100 throughout the entire time period was $710\,\mathrm{cm^{-3}}$. Our estimate of regional-scale boundary-layer new-particle formation to N100 is thus 56 %. This estimate is larger than our predicted contribution of regional-scale boundary-layer new-particle formation to N50 (40 %). Primary emissions will con-

ACPD
14, 707–750, 2014

tribute to a larger fraction of the particles with increasing size, so our result is not physical. There are three reasons why our $N100_{NPF}$ calculation may be too high relative to our $N50_{NPF}$ calculation: (1) the lifetime of 100 nm particles is likely shorter than 50 nm particles as 100 nm particles will act as CCN in a larger fraction of clouds, and thus 100 nm particles are more susceptible to wet deposition. (2) The boundary layer may have grown in depth between the time the nucleation mode reached 50 nm and when it reached 100 nm. (3) The 2 highest SP100 days shift the mean SP100 (19 %) significantly above the median (7 %). If we had a larger sample of event days, it is possible that the mean would be closer to the median, and the fractional contribution of new-particle formation to 100 nm particles would be lower than the fractional contribution of new-particle formation to 50 nm particles.

These estimated contributions of new-particle formation to CCN-sized particles (40–56 %) is similar to the global boundary-layer contribution of new-particle formation to CCN-sized particles estimated in the modelling study by Merikanto et al. (2009); however, they found that much of this contribution was due to new-particle formation in the free troposphere (with subsequent subsidence into the boundary layer) rather than boundary-layer new-particle formation.

3.2 Conditions during new-particle formation events

Figure 4 shows box-whisker plots for the atmospheric conditions on each type of event and non-event day. For event days, the values for each variable are taken as the mean value between the start and end of new-particle formation (the period where new particles are arriving at diameters of ∼ 10 nm). For non-event days, the values for each variable are the 24 h mean of the day since there is no new-particle-formation event time to draw upon. We display the statistical significance of differences between the distributions of each event class using the Mann–Whitney U test. Although not shown on the plots, the distributions for 1a days are statistically different from non-event days to at least the 98 % level for all factors except condensation sink (89 %).

Discussion Paper | Discussion Paper | Discussion Paper | Discussion Paper |

ACPD

14, 707–750, 2014

Solar radiation drives photochemistry and thus the oxidation of SO_2 to form condensible H_2SO_4 and volatile organic compounds to form condensible organic species. Previous studies (e.g. Petäjä et al., 2009) have shown new-particle formation events to be strongly correlated with solar radiation. Solar radiation on class 1a and 1b days were significantly higher than class 2 and non-event days. All 1a events occurred between 7 a.m. and 7 p.m. LST, and all but 2 (out of 57) 1b events occurred during this time window (not shown). On the other hand 15 (out of 164) class 2 events occurred outside of this window (not shown), and the non-event solar radiation stats are 24 h averaged. These time-of-day differences explain part of the differences in solar radiation; however, differences in large-scale meteorology (and their effects on cloud cover) between event days were likely important too, as will be shown shortly. Class 1a days have higher solar radiation than 1b days, on average, though the statistical difference is just short of being significant to the 95 % level (94.7 %). Thus, similar to the previous studies, the amount of solar radiation likely plays a role in initiating regional-scale new-particle formation events, and nighttime chemistry appears to be less important as 1a and 1b events generally do not occur during dark hours.

While some nucleation theories (e.g. Vehkamäki et al., 2002) predict increased nucleation rates with relative humidity, the data (as well as other observations) show a general anti-correlation between nucleation and relative humidity (relative humidity generally increases moving from class 1a to 1b to 2 to non-events). This increase in relative humidity is likely not causally linked to the likelihood of regional-scale new-particle formation events, rather (1) clouds are more likely when the relative humidity is higher, (2) the relative humidity is generally higher at night (and would bias class 2 events and the non-events higher), and (3) the condensation sink generally increases with relative humidity due to aerosol water uptake. While the difference in relative humidity between class 1a and 1b events with class 2 events and non-events is statistically significant, the difference between the 1a and 1b events is not.

Temperature anomalies (difference of the event-time temperature from the 4 week running mean) were mostly positive for class 1a days (75 % of the events) and the data

ACPD
14, 707–750, 2014

show a decreasing trend moving from class 1a to 1b to 2 to non-events; however, the difference between successive classes are not significant to the 95 % level (though the difference between class 1a events class 2 events or non-events is significant). The cause of the higher mean/median temperature anomaly on class 1a days may be due to clear skies from large-scale meteorology and is consistent with the solar-radiation and relative humidity statistics (as will be discussed in the next subsection).

Surface pressure anomalies (also the difference of the event-time pressure from the 4 week running mean) also were mostly positive for class 1a days (75 % of the events) with decreasing values moving from class 1a to 1b to 2 to non-events. Differences between class 1a and class 1b events are not statistically significant, whereas the differences between these event classes with class 2 and non-event days are statistically significant. The positive surface pressure anomaly for ∼ 75 % of the class 1a and slightly less than 75 % of the class 1b events shows that large-scale synoptic meteorology may have played a role in driving many of the regional-scale new-particle formation events. Surface highs in the mid-latitudes are associated with large-scale subsidence in the free troposphere, clear skies and lower-than-normal relative humidities. We will look regionally at differences in large-scale meteorology in the next subsection.

The condensation sink is the rate constant for condensation of a non-volatile condensible species from the vapor phase to the particle phase. Lower condensation sinks favor new-particle formation and growth because concentrations of condensible species may build up and lead to faster nucleation and growth rates. This has been observed in previous studies (e.g. Petäjä et al. (2009); Sihto et al., 2006). However, we find that class 1a event days had, on average, the highest condensation sinks. The condensation sinks on class 1a days were significantly higher than class 1a and 1b days (though not significantly higher than non-event days). This means that on the days most likely to have regional nucleation and growth at Egbert, the condensation sink was higher than on other days. A higher condensation sink must be offset by a high production rate of low-volatility condensible material (e.g. H_2SO_4 and low-volatility organics) to create favorable conditions for new-particle formation and growth. As we discuss in the next

ACPD
14, 707–750, 2014

subsection, the high condensation-sink days generally occurred when air arrived from the heavily populated region to the south of Egbert.

The concentrations of SO_2, the precursor to condensible H_2SO_4 vapor, were highest on average on class 1a event days followed by class 1b, class 2 and non-event days. Class 1a days were not significantly higher (only 88.6 % significant) than class 1b days, but they were significantly higher than class 2 and non-event days. Class 2 event days however, had 4 high-concentration outliers that were higher than all of the class 1a and 1b points. These class-2-event results may be indicative of plume-scale nucleation in a coal-fired power-plant some other sulfur-rich plume (Junkermann et al., 2011; Lonsdale et al., 2012; Stevens et al., 2012; Yu, 2010). In the next subsection, we will show that the higher SO_2 days generally occur when air arrives from the heavily populated region to the south of Egbert, similar to the condensation sink.

Finally, we use a proxy for H_2SO_4 concentration (Petäjä et al., 2009; Rohrer and Berresheim, 2006; Weber et al., 1997) to determine if H_2SO_4 concentrations were higher during regional nucleation events than during other days. The proxy we use is:

$$[H_2SO_4] \propto \frac{SR \cdot [SO_2]}{CS} \quad (2)$$

Where SR is the solar radiation and CS is the condensation sink. Note, we have plotted this proxy on log scale due to the wide range of values. Although the condensation sink was highest on average for class 1a events, the H_2SO_4 proxy was highest on average for class 1a days because both SR and CS were highest on average for these days. The distribution of the H_2SO_4 proxy is not significantly different at the 95 % level (but is at the 90 % level) from class 1b days (partly because of the higher mean and median, and partly because of the broader distribution). Class 1a days were statistically different from class 2 and non-event days, with higher means and medians.

Unfortunately, we do not have measurements of organics throughout the time period used here, so we are limited to information on sulfuric acid. However, emissions of biogenic volatile organic compounds (precursors for secondary organics that may contribute to nucleation and growth, Riipinen et al., 2011, 2012) are more favorable under

ACPD
14, 707–750, 2014

warmer and sunnier conditions at Egbert (Leaitch et al., 2011) and elsewhere (Paasonen et al., 2013) and thus lead to organic aerosol formation under these conditions. Because class 1a events had the highest amount of solar radiation and temperature anomalies on average, condensation of low-volatility organic vapors to a growing nucleation mode may be more favorable on these days.

While Fig. 4 shows the distributions of environmental factors during events in the various classes, it does not show how new-particle-formation rates (J10) or growth rates (GR) vary with the values of these factors. Table 2 shows the correlation coefficients of J10 and GR with the 7 environmental factors in Fig. 4 on class 1a days. Because J10s and GRs span several orders of magnitude we take the log of these as well as the log of condensation sink, SO_2 and the H_2SO_4 proxy, which each span orders of magnitude. All of the environmental factors show stronger correlations (or anti-correlations) with J10 than with the GRs. This could be because other, independent factors (e.g. the condensation of low-volatility organics) may be more important to GRs than to J10s. As would be expected, J10 is positively correlated with solar radiation, SO_2 and the H_2SO_4 proxy (albeit weakly). Oddly, J10 is also positively correlated with the condensation sink. However, the condensation sink is also positively correlated with SO_2 (correlation coefficient = 0.74, not shown), which offsets the dampening effect of condensation sink and leads to the weak positive correlation with the H_2SO_4 proxy. Because the correlation of the H_2SO_4 proxy with J10 is weak, it is likely that other species (e.g. organics) are contributing to J10s also.

3.3 Large-scale meteorology and back trajectories

In this section, we look at the regional meteorological features associated with the different types of events. Figure 5 shows the surface pressure anomaly (differences from the 4-week running mean centered on the event day) for the mean of class 1a, 1b and 2 event days. Regions with a statistically significant high surface pressure anomaly are shaded in pink, and regions where there is a statistically significant low surface pressure anomaly are shaded in blue. Statistical significance is computed following the

Discussion Paper | Discussion Paper | Discussion Paper | Discussion Paper |

ACPD
14, 707–750, 2014

New-particle formation, growth and climate-relevant particle production

J. R. Pierce et al.

bootstrap method (Efron, 1979; see Appendix A for details). Consistent with the high surface-pressure anomalies on class 1a event days measured at Egbert in Fig. 4c, the entire region around Egbert had a surface pressure anomaly of more than 300 Pa and this high anomaly was statistically significant to the 95 % level. Although not shown in Fig. 5, Egbert is located inside a region with a 99.8 % significant high anomaly. We note that not all of the 44 class 1a events exhibited anomalous high pressure over Egbert. 25 % of the class 1a event days experienced low pressure anomalies at the site (Fig. 4c). Class 1b events also exhibited a positive surface pressure anomaly (150 hPa), but no regions were statistically significant to the 95 % level. For Class 2 events, the composite meteorological surface pressure pattern was markedly different from that for 1a and 1b events (Fig. 5c). For Class 2 events, the region of higher surface pressure was located northeast of Egbert, with a region of low surface pressure to the southwest.

Figure 6 shows composites of the full 500 hPa geopotential height field (i.e. the anomalies have been added back to the mean). The pink and blue areas show the regions of the statistically significant anomalies. There was a statistically significant geopotential height anomaly on class 1a days west of Egbert, placing Egbert to the east of the ridge. The east sides of the 500 hPa geopotential ridges are associated with tropospheric subsidence and surface highs, consistent with Fig. 5. There are no significant height anomalies in the vicinity of Egbert for the class 1b or class 2 days.

We also looked at the large-scale vertical velocity (omega) fields from NCEP (not shown), and consistent with the large-scale dynamics shown in Figs. 5 and 6, the class 1a days had a statistically significant subsidence over and around Egbert. Class 1b days have subsidence over Egbert too, but it was not statistically significant. Class 2 days had no major vertical-wind structure.

The NCEP analysis that we have done here shows that the regional-scale new-particle formation events (class 1a) are often associated with the large-scale synoptic pattern with surface highs, large-scale and a ridge to the west and a trough to the east of Egbert. This is not entirely surprising since these conditions generally bring sunny

ACPD
14, 707–750, 2014

conditions over the region of subsidence and allow for a homogeneous boundary layer (assuming somewhat spatially homogeneous emissions). These large-scale conditions may explain the measured solar radiation, relative humidity, temperature anomaly and pressure anomaly presented in Fig. 4; however, it is not clear if these conditions also drive the surface-wind directions associated with the high condensation sink and SO_2 concentration seen in class 1a days in Fig. 4. To explore this, we use HYPLIT back trajectories.

Figure 7 shows one 24 h HYSPLIT back trajectory for each new-particle formation event from the three event classes. The trajectory from each event ends at the hour closest to the middle of the new-particle formation event. The trajectories are colored by the SO_2 mixing ratio during the new-particle formation event. There does not appear to have been a dominant wind direction to Egbert for any of the new-particle-formation event classes. However, for all event classes, higher SO_2 air generally came from the densely populated regions from the south with lower SO_2 air generally from the north. Each event class had cases with both lower and higher SO_2 air.

Figure 8 shows the same back trajectories but color coded by the condensation sink. The directional dependence of the condensation sink was very similar to that of SO_2. Thus, air from the south had both high SO_2 and high condensation sink on new-particle formation days for all event classes, which is consistent with earlier studies at Egbert that found that polluted air most often is from the South (Rupakheti et al., 2005). These results are consistent with the correlation coefficient between SO_2 and condensation sink of 0.74 on class 1a days discussed earlier. Interestingly, the regional-scale nucleation events (class 1a and maybe class 1b) were roughly equally likely to occur in clean vs. polluted air, which may have been due to the opposing effects of SO_2 and the condensation sink on new-particle formation.

Figures 9 and 10 show the same back trajectories but color coded by the pressure anomaly and solar radiation, respectively. The figures show that the high pressure-anomaly and high solar-radiation days were generally associated with air flowing to Egbert from the east and north. (The class 2 days have some low solar-radiation events

ACPD
14, 707–750, 2014

from all directions due to nighttime events.) Thus, the days with high pressure and solar radiation were generally different from the high SO_2 and condensation-sink (though there was some overlap between high pollution and high solar radiation on days coming from the southeast on class 1a days).

Taking into account all of the analyses in Sects. 3.2 and 3.3, it appears that regional-scale new-particle formation (class 1a and possibly class 1b events) occurred under 2 different sets of conditions (1) days with the large-scale synoptic meterology shown in Figs. 5 and 6 with high surface pressure, large-scale subsidence and clear skies generally driving airflow from the clean regions, and (2) days with polluted (yet relatively homogeneously mixed) air flow from the south. For some cases when air was coming from the southeast, both of these conditions were satisfied and the air was both polluted and had the favorable synoptic conditions. These two conditions for new-particle formation in the region near Egbert was also noted in (Jeong et al., 2010), who looked at new-particle formation at Egbert and three other sites in Southern Ontario for three weeks during the summer of 2007. As shown in Table 2, J10 and growth rates were correlated with SO_2 and CS, which means that the regional new-particle events occurring in the polluted events from the south were generally more intense than the events occurring in the cleaner air from the north.

4 Conclusions

In this paper, we use one year of aerosol size measurements at Egbert, ON, Canada to explore new-particle formation and growth to climate-relevant particle sizes at this site. We present both the statistics of formation rates, growth rates and survival probabilities as well as an analysis of the factors that may have contributed to the new-particle formation and growth. We find that the regional-scale new-particle formation event frequency peaked in the spring and fall (30–50 % of the days) with minima in the winter and summer. The winter minimum may have been due to a lack of biogenic organic precursors to nucleation and growth and lower solar radiation while the summer had lower SO_2 mixing ratios than the other seasons.

Observed new-particle formation rates ranged from less than 0.1 to close to 10 $cm^{-3}\,s^{-1}$ during the events, or about 5–10 times lower when averaged over the event day. The 24 h mean and median values, 0.13 and 0.12 $cm^{-3}\,s^{-1}$, were within the range of values found at 5 sites investigated by Westervelt et al. (2013). Growth rates ranged from less than 0.5 to over 10 $nm\,h^{-1}$ with mean and median values of 3.1 and 2.0 $nm\,h^{-1}$, also within the range of Westervelt et al. (2013). The survival probabilities of growth to 50 and 100 nm (SP50 and SP100) ranged from less than 1 % to over 90 %. The mean and median values for SP50 (33 % and 19 %) are consistent with the sites in Westervelt et al. (2013), but the values for SP100 (19 % and 7 %) are higher than the sites in Westervelt et al. (2013).

We estimate that the mean formation rate of 50 and 100 nm particles on regional new-particle formation days were 0.039 and 0.022 $cm^{-3}\,s^{-1}$ (averaged over the full day). From this, we estimate that regional new-particle formation events contributed about half of the climate-relevant particles; however, there is significant uncertainty in our calculation due to uncertainties in aerosol lifetime and changes in the boundary-layer height.

We find that regional new-particle formation events often occurred under synoptic conditions associated with high surface pressure and large-scale subsidence that cause sunny conditions and clean-air flow from the north and west. However, new-particle formation also occurred when air flow came from the polluted regions to the south and southwest of Egbert. This air is associated with high SO_2 concentrations and high aerosol condensation sinks. The nucleation rates tended to be faster during events under these south/southwest flow conditions.

A major factor missing from this analysis is the formation rates of secondary organic aerosol (SOA). SOA may form from biogenic volatile organic compounds emitted by vegetation in the region around Egbert or through anthropogenic volatile organic compounds emitted from industry to the south of Egbert. SOA has been shown to

ACPD
14, 707–750, 2014

be a contributor to both particle formation and growth (Donahue et al., 2011; Metzger et al., 2010; Pierce et al., 2011; Riipinen et al., 2011), and thus variability in SOA formation rates very likely contributed to some of the variability in new-particle formation occurrence, new-particle formation rates, growth rates and survival probabilities. However, we do not have measurements of aerosol composition or of SOA precursor gases for most of the time period explored in this paper and thus do not include it here.

This work provides valuable statistical constraints for testing model predictions of new-particle formation and growth rates (and the driving factors for these rates) at Egbert. Future work will involve comparing the statistics of new-particle formation, growth rates and survival probabilities of an aerosol microphysics model, such as GEOS-Chem-TOMAS, to the measured statistics shown here similar to what was done in Westervelt et al. (2013). Additionally, we can test to see if the meteorological and background chemical factors (e.g. SO_2) are similar in the simulations as to the measurements. These comparisons will allow a comprehensive test of modeled nucleation and condensational growth schemes.

Appendix A

Statistical significance of meteorological patterns

The statistical significance of the meteorological patterns in Figs. 5 and 6 are computed using the Bootstrap method (Efron, 1979) to determine if regional-scale new-particle formation events (class 1a events and possibly class 1b events) were associated with distinct regional meteorology. We summarize the bootstrap method here. We create 10 000 sets of 44 randomly sampled days (the number of class 1a days; 57 days for class 1b events and 164 for class 2 events) of surface pressure anomalies, 500 hPa height anomalies and vertical wind anomalies from the NCEP database (from between 1997 and 2009) over the region shown in Figs. 5 and 6. Like in Fig. 4c and d, the anomalies are defined as differences from the 4-week running mean centered on the

ACPD
14, 707–750, 2014

event day. We calculate the mean anomalies at each grid point for each of the 10 000 sets. Then, at each location, if the observed anomaly falls outside of the 2.5th–97.5th percentile range (confidence interval) of the 10 000 sample-set, we say that the observed anomaly is statistically significant at 95 % confidence using a two-tailed test.

Acknowledgements. Funding was provided through Environment Canada's Grants and Contribution program (G&C 1300358).

References

Boy, M., Kulmala, M., Ruuskanen, T. M., Pihlatie, M., Reissell, A., Aalto, P. P., Keronen, P., Dal Maso, M., Hellen, H., Hakola, H., Jansson, R., Hanke, M., and Arnold, F.: Sulphuric acid closure and contribution to nucleation mode particle growth, Atmos. Chem. Phys., 5, 863–878, doi:10.5194/acp-5-863-2005, 2005.

Charlson, R. J., Schwartz, S. E., Hales, J. M., Cess, R. D., Coakley, J. A., Hansen, J. E., and Hofman, D. J.: Climate forcing by anthropogenic aerosols, Science, 255, 423–430, 1992.

Crippa, P. and Pryor, S. C.: Spatial and temporal scales of new particle formation events in eastern North America, Atmos. Environ., 75, 257–264, 2013.

Croft, B., Pierce, J. R., and Martin, R. V.: Interpreting aerosol lifetimes using the GEOS-Chem model and constraints from radionuclide measurements, Atmos. Chem. Phys. Discuss., 13, 32391–32421, doi:10.5194/acpd-13-32391-2013, 2013.

Dal Maso, M., Kulmala, M., Dal Maso, M., Riipinen, I., Wagner, R., Hussein, T., Aalto, P., and Lehtinen, K. E. J.: Formation and growth of fresh atmospheric aerosols: eight years of aerosol size distribution data from SMEAR II, Hyytiala, Finland, Boreal Env. Res., 10, 323–336, 2005.

Donahue, N. M., Trump, E. R., Pierce, J. R., and Riipinen, I.: Theoretical constraints on pure vapor-pressure driven condensation of organics to ultrafine particles, Geophys. Res. Lett., 38, L16801, doi:10.1029/2011GL048115, 2011.

Draxler, R.: HYSPLIT4 User's Guide, NOAA Tech. Memo. ERL ARL-230, Silver Spring, MD, 1999.

Draxler, R. R. and Hess, G. D.: Description of the HYSPLIT_4 modeling system, NOAA Tech. Memo. ERL ARL-224, NOAA Air Resources Laboratory, Silver Spring, MD, 24 pp., 1997.

Draxler, R. R. and Hess, G. D.: An overview of the HYSPLIT_4 modeling system of trajectories, dispersion, and deposition, Aust. Meteorol. Mag., 47, 295–308, 1998.

Dusek, U., Frank, G. P., Hildebrandt, L., Curtius, J., Schneider, J., Walter, S., Chand, D., Drewnick, F., Hings, S., Jung, D., Borrmann, S., and Andreae, M. O.: Size matters more than chemistry for cloud-nucleating ability of aerosol particles, Science, 312, 1375–1378, 2006.

Efron, B.: Bootstrap methods: another look at the jackknife, Ann. Stat., 7, 1–26, 1979.

Forster, P., Ramaswamy, V., Artaxo, P., Berntsen, T., Betts, R., Fahey, D. W., Haywood, J., Lean, J., Lowe, D. C., Myhre, G., Nganga, J., Prinn, R., Raga, G., Schulz, M., and Dorland, R. V.: Changes in atmospheric constituents and in radiative forcing, in: Climate Change 2007: The Physical Science Basis. Contribution of Working Group I to the Fourth Assessment Report of the Intergovernmental Panel on Climate Change, edited by: Solomon, S., Qin, D., Manning, M., Chen, Z., Marquis, M., Averyt, K. B., Tignor, M., and Miller, H. L., Cambridge University Press, Cambridge, UK and New York, NY, USA, 129–234, 2007.

Jeong, C.-H., Evans, G. J., McGuire, M. L., Chang, R. Y.-W., Abbatt, J. P. D., Zeromskiene, K., Mozurkewich, M., Li, S.-M., and Leaitch, W. R.: Particle formation and growth at five rural and urban sites, Atmos. Chem. Phys., 10, 7979–7995, doi:10.5194/acp-10-7979-2010, 2010.

Junkermann, W., Vogel, B., and Sutton, M. A.: The climate penalty for clean fossil fuel combustion, Atmos. Chem. Phys., 11, 12917–12924, doi:10.5194/acp-11-12917-2011, 2011.

Kalnay, E., Kanamitsu, M., Kistler, R., Collins, W., Deaven, D., Gandin, L., Iredell, M., Saha, S., White, G., Woollen, J., Zhu, Y., Leetmaa, A., Reynolds, R., Chelliah, M., Ebisuzaki, W., Higgins, W., Janowiak, J., Mo, K. C., Ropelewski, C., Wang, J., Jenne, R., and Joseph, D.: The NCEP/NCAR 40 yr reanalysis project, B. Am. Meteorol. Soc., 77, 437–471, doi:10.1175/1520-0477(1996)077<0437:TNYRP>2.0.CO;2, 1996.

Kerminen, V.-M., Paramonov, M., Anttila, T., Riipinen, I., Fountoukis, C., Korhonen, H., Asmi, E., Laakso, L., Lihavainen, H., Swietlicki, E., Svenningsson, B., Asmi, A., Pandis, S. N., Kulmala, M., and Petäjä, T.: Cloud condensation nuclei production associated with atmospheric nucleation: a synthesis based on existing literature and new results, Atmos. Chem. Phys., 12, 12037–12059, doi:10.5194/acp-12-12037-2012, 2012.

Kuang, C., McMurry, P. H., and McCormick, A. V: Determination of cloud condensation nuclei production from measured new particle formation events, Geophys. Res. Lett., 36, L09822, doi:10.1029/2009GL037584, 2009.

Kuang, C., Chen, M., Zhao, J., Smith, J., McMurry, P. H., and Wang, J.: Size and time-resolved growth rate measurements of 1 to 5 nm freshly formed atmospheric nuclei, Atmos. Chem. Phys., 12, 3573–3589, doi:10.5194/acp-12-3573-2012, 2012.

Kulmala, M., Vehkamaki, H., Petajda, T., Dal Maso, M., Lauri, A., Kerminen, V. M., Birmili, W., and McMurry, P. H.: Formation and growth rates of ultrafine atmospheric particles: a review of observations, J. Aerosol Sci., 35, 143–176, 2004.

Kulmala, M., Petäjä, T., Mönkkönen, P., Koponen, I. K., Dal Maso, M., Aalto, P. P., Lehtinen, K. E. J., and Kerminen, V.-M.: On the growth of nucleation mode particles: source rates of condensable vapor in polluted and clean environments, Atmos. Chem. Phys., 5, 409–416, doi:10.5194/acp-5-409-2005, 2005.

Leaitch, W. R., Macdonald, A. M., Brickell, P. C., Liggio, J., Sjostedt, S. J., Vlasenko, A., Bottenheim, J. W., Huang, L., Li, S.-M., Liu, P. S. K., Toom-Sauntry, D., Hayden, K. A., Sharma, S., Shantz, N. C., Wiebe, H. A., Zhang, W., Abbatt, J. P. D., Slowik, J. G., Chang, R. Y.-W., Russell, L. M., Schwartz, R. E., Takahama, S., Jayne, J. T., and Ng, N. L.: Temperature response of the submicron organic aerosol from temperate forests, Atmos. Environ. 45, 6696–6704, 2011.

Lonsdale, C. R., Stevens, R. G., Brock, C. A., Makar, P. A., Knipping, E. M., and Pierce, J. R.: The effect of coal-fired power-plant SO_2 and NO_x control technologies on aerosol nucleation in the source plumes, Atmos. Chem. Phys., 12, 11519–11531, doi:10.5194/acp-12-11519-2012, 2012.

Merikanto, J., Spracklen, D. V., Mann, G. W., Pickering, S. J., and Carslaw, K. S.: Impact of nucleation on global CCN, Atmos. Chem. Phys., 9, 8601–8616, doi:10.5194/acp-9-8601-2009, 2009.

Metzger, A., Verheggen, B., Dommen, J., Duplissy, J., Prevot, A. S. H., Weingartner, E., Riipinen, I., Kulmala, M., Spracklen, D. V, Carslaw, K. S., and Baltensperger, U.: Evidence for the role of organics in aerosol particle formation under atmospheric conditions, P. Natl. Acad. Sci. USA, 107, 6646–6651, doi:10.1073/pnas.0911330107, 2010.

Paasonen, P., Asmi, A., Petäjä, T., Kajos, M. K., Äijälä, M., Junninen, H., Holst, T., Abbatt, J. P. D., Arneth, A., Birmili, W., van der Gon, H. D., Hamed, A., Hoffer, A., Laakso, L., Laaksonen, A., Richard Leaitch, W., Plass-Dülmer, C., Pryor, S. C., Räisänen, P., Swietlicki, E., Wiedensohler, A., Worsnop, D. R., Kerminen, V.-M., and Kulmala, M.: Warming-induced increase in aerosol number concentration likely to moderate climate change, Nat. Geosci., 6, 438–442, doi:10.1038/ngeo1800, 2013.

Paramonov, M., Aalto, P. P., Asmi, A., Prisle, N., Kerminen, V.-M., Kulmala, M., and Petäjä, T.: The analysis of size-segregated cloud condensation nuclei counter (CCNC) data and its implications for cloud droplet activation, Atmos. Chem. Phys., 13, 10285–10301, doi:10.5194/acp-13-10285-2013, 2013.

Petäjä, T., Mauldin, III, R. L., Kosciuch, E., McGrath, J., Nieminen, T., Paasonen, P., Boy, M., Adamov, A., Kotiaho, T., and Kulmala, M.: Sulfuric acid and OH concentrations in a boreal forest site, Atmos. Chem. Phys., 9, 7435–7448, doi:10.5194/acp-9-7435-2009, 2009.

Pierce, J. R. and Adams, P. J.: Efficiency of cloud condensation nuclei formation from ultrafine particles, Atmos. Chem. Phys., 7, 1367–1379, doi:10.5194/acp-7-1367-2007, 2007.

Pierce, J. R. and Adams, P. J.: Uncertainty in global CCN concentrations from uncertain aerosol nucleation and primary emission rates, Atmos. Chem. Phys., 9, 1339–1356, doi:10.5194/acp-9-1339-2009, 2009.

Pierce, J. R., Riipinen, I., Kulmala, M., Ehn, M., Petäjä, T., Junninen, H., Worsnop, D. R., and Donahue, N. M.: Quantification of the volatility of secondary organic compounds in ultrafine particles during nucleation events, Atmos. Chem. Phys., 11, 9019–9036, doi:10.5194/acp-11-9019-2011, 2011.

Pierce, J. R., Leaitch, W. R., Liggio, J., Westervelt, D. M., Wainwright, C. D., Abbatt, J. P. D., Ahlm, L., Al-Basheer, W., Cziczo, D. J., Hayden, K. L., Lee, A. K. Y., Li, S.-M., Russell, L. M., Sjostedt, S. J., Strawbridge, K. B., Travis, M., Vlasenko, A., Wentzell, J. J. B., Wiebe, H. A., Wong, J. P. S., and Macdonald, A. M.: Nucleation and condensational growth to CCN sizes during a sustained pristine biogenic SOA event in a forested mountain valley, Atmos. Chem. Phys., 12, 3147–3163, doi:10.5194/acp-12-3147-2012, 2012.

Riipinen, I., Pierce, J. R., Yli-Juuti, T., Nieminen, T., Häkkinen, S., Ehn, M., Junninen, H., Lehtipalo, K., Petäjä, T., Slowik, J., Chang, R., Shantz, N. C., Abbatt, J., Leaitch, W. R., Kerminen, V.-M., Worsnop, D. R., Pandis, S. N., Donahue, N. M., and Kulmala, M.: Organic condensation: a vital link connecting aerosol formation to cloud condensation nuclei (CCN) concentrations, Atmos. Chem. Phys., 11, 3865–3878, doi:10.5194/acp-11-3865-2011, 2011.

Riipinen, I., Yli-Juuti, T., Pierce, J. R., Petäjä, T., Worsnop, D. R., Kulmala, M., and Donahue, N. M.: The contribution of organics to atmospheric nanoparticle growth, Nat. Geosci., 5, 453–458, doi:10.1038/ngeo1499, 2012.

Rohrer, F. and Berresheim, H.: Strong correlation between levels of tropospheric hydroxyl radicals and solar ultraviolet radiation, Nature, 442, 184–187, doi:10.1038/nature04924, 2006.

Rupakheti, M., Leaitch, W. R., Lohmann, U., Hayden, K., Brickell, P., Lu, G., Li, S.-M., Toom-Sauntry, D., Bottenheim, J. W., Brook, J. R., Vet, R., Jayne, J. T., and Worsnop, D. R.: An intensive study of the size and composition of submicron atmospheric aerosols at a rural site in Ontario, Canada, Aerosol Sci. Tech., 39, 722–736, doi:10.1080/02786820500182420, 2005.

Seinfeld, J. H. and Pandis, S. N.: Atmospheric Chemistry and Physics, 1st edn., John Wiley and Sons, New York, 2006.

Sihto, S.-L., Kulmala, M., Kerminen, V.-M., Dal Maso, M., Petäjä, T., Riipinen, I., Korhonen, H., Arnold, F., Janson, R., Boy, M., Laaksonen, A., and Lehtinen, K. E. J.: Atmospheric sulphuric acid and aerosol formation: implications from atmospheric measurements for nucleation and early growth mechanisms, Atmos. Chem. Phys., 6, 4079–4091, doi:10.5194/acp-6-4079-2006, 2006.

Slowik, J. G., Stroud, C., Bottenheim, J. W., Brickell, P. C., Chang, R. Y.-W., Liggio, J., Makar, P. A., Martin, R. V., Moran, M. D., Shantz, N. C., Sjostedt, S. J., van Donkelaar, A., Vlasenko, A., Wiebe, H. A., Xia, A. G., Zhang, J., Leaitch, W. R., and Abbatt, J. P. D.: Characterization of a large biogenic secondary organic aerosol event from eastern Canadian forests, Atmos. Chem. Phys., 10, 2825–2845, doi:10.5194/acp-10-2825-2010, 2010.

Spracklen, D. V., Carslaw, K. S., Kulmala, M., Kerminen, V.-M., Mann, G. W., and Sihto, S.-L.: The contribution of boundary layer nucleation events to total particle concentrations on regional and global scales, Atmos. Chem. Phys., 6, 5631–5648, doi:10.5194/acp-6-5631-2006, 2006.

Stevens, R. G. and Pierce, J. R.: A parameterization of sub-grid particle formation in sulphur-rich plumes for global and regional-scale models, Atmos. Chem. Phys. Discuss., 13, 19583–19623, doi:10.5194/acpd-13-19583-2013, 2013.

Stevens, R. G., Pierce, J. R., Brock, C. A., Reed, M. K., Crawford, J. H., Holloway, J. S., Ryerson, T. B., Huey, L. G., and Nowak, J. B.: Nucleation and growth of sulfate aerosol in coal-fired power plant plumes: sensitivity to background aerosol and meteorology, Atmos. Chem. Phys., 12, 189–206, doi:10.5194/acp-12-189-2012, 2012.

Vehkamäki, H., Kulmala, M., Napari, I., Lehtinen, K. E. J., Timmreck, C., Noppel, M., and Laaksonen, A.: An improved parameterization for sulfuric acid-water nucleation rates for tropospheric and stratospheric conditions, J. Geophys. Res., 107, 4610–4622, 2002.

ACPD
14, 707–750, 2014

Weber, R. J., Marti, J. J., McMurry, P. H., Eisele, F. L., Tanner, D. J., and Jefferson, A.: Measurements of new particle formation and ultrafine particle growth rates at a clean continental site, J. Geophys. Res., 102, 4375–4385, 1997.
Westervelt, D. M., Pierce, J. R., Riipinen, I., Trivitayanurak, W., Hamed, A., Kulmala, M., Laaksonen, A., Decesari, S., and Adams, P. J.: Formation and growth of nucleated particles into cloud condensation nuclei: model–measurement comparison, Atmos. Chem. Phys., 13, 7645–7663, doi:10.5194/acp-13-7645-2013, 2013.
Yu, F.: Diurnal and seasonal variations of ultrafine particle formation in anthropogenic SO_2 plumes, Environ. Sci. Technol., 44, 2011–2015, doi:10.1021/es903228a, 2010.

ACPD
14, 707–750, 2014

Table 1. Means and medians of nucleation, growth and CCN-formation parameters across all days of each event class.

Class	# of days	J10 $cm^{-3}\,s^{-1}$	J10 (24 h) $cm^{-3}\,s^{-1}$	GR $nm\,h^{-1}$	SP50 %	SP100 %	J50 (24 h) $cm^{-3}\,s^{-1}$	J100 (24 h) $cm^{-3}\,s^{-1}$
1a (means)	44	0.84	0.13	3.1	33	19	0.039	0.022
1a (medians)	44	0.64	0.12	2.4	19	7	0.029	0.0091
1b (means)	57	0.58	0.069	3.1	N/A	N/A	N/A	N/A
1b (medians)	57	0.22	0.049	2.0	N/A	N/A	N/A	N/A
1a + 1b (means)	101	0.69	0.097	3.1	N/A	N/A	N/A	N/A
1a + 1b (medians)	101	0.30	0.050	2.2	N/A	N/A	N/A	N/A

ACPD
14, 707–750, 2014

Table 2. Correlation coefficients between environmental factors with J10s and GRs on class 1a days.

	log(J10)	log(GR)
Solar radiation	0.42	0.06
RH	−0.26	0.10
T anomaly	0.27	0.16
P anomaly	−0.14	−0.03
log(Condensation sink)	0.44	0.18
log(SO_2 mixing ratio)	0.33	0.23
log($SR \cdot SO_2/CS$)	0.20	0.12

ACPD
14, 707–750, 2014

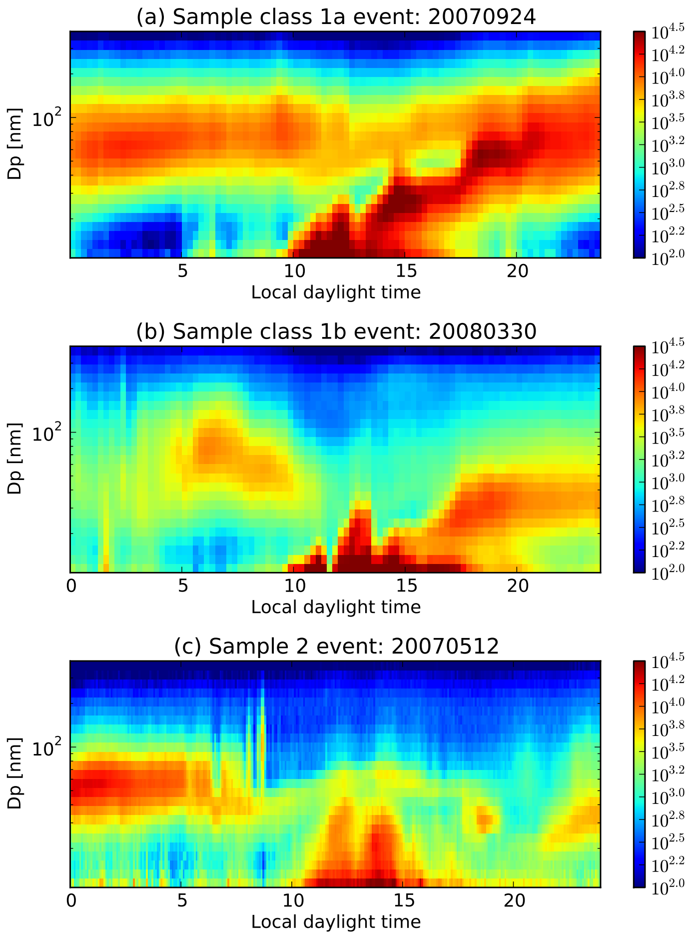

Fig. 1. Sample size-distribution time series for a **(a)** class 1a nucleation day, **(b)** class 1b nucleation day and **(c)** class 2 nucleation day. The color axis is $dN/d\log D_p$ [cm^{-3}].

ACPD
14, 707–750, 2014

New-particle formation, growth and climate-relevant particle production

J. R. Pierce et al.

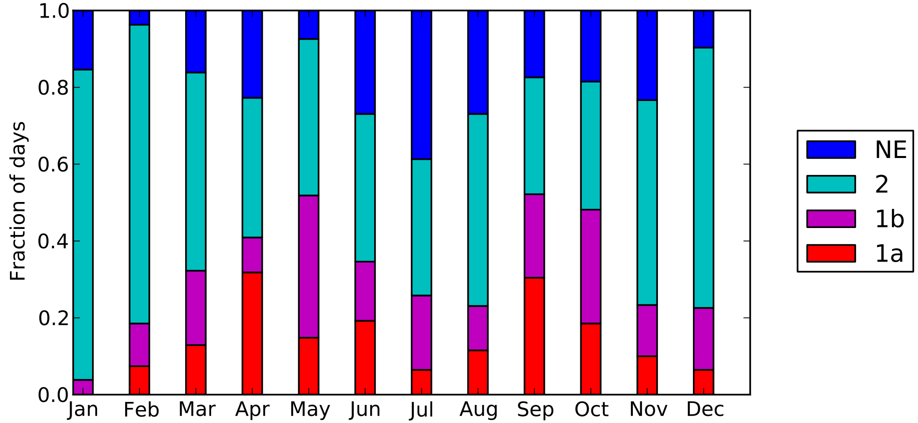

Fig. 2. The fraction of days in each month classified as having class 1a, 1b and 2 events as well as days with no events (NE). Some days did not have at least 75 % of the day with SMPS data and were not used. All months had at least 22 classified days. Note that multiple class 2 events may occur on a given class 2 event day. Class 2 events may also occur on class 1a or class 1b event days; however, these are counted as 1a or 1b days.

ACPD
14, 707–750, 2014

New-particle formation, growth and climate-relevant particle production

J. R. Pierce et al.

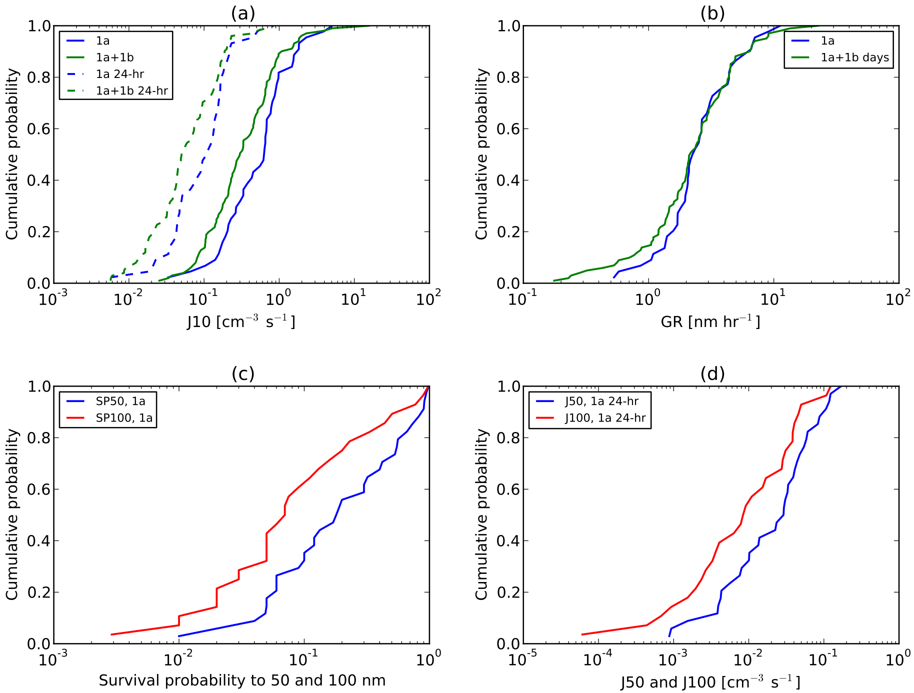

Fig. 3. Cumulative probability distributions of various nucleation and growth metrics from the full year. **(a)** J10 rates for both 1a days and 1a + 1b days. Solid lines show the rates averaged only over the period where nucleation was occurring. Dashed lines show the rates averaged over the full day. **(b)** Growth rates for both 1a days and 1a + 1b days. For the following panels, only 1a days are shown as we do not trust the estimates of survival probability for 1b days. **(c)** Survival probability to 50 and 100 nm. **(e)** 24 h-mean production rate of 50 and 100 nm particles.

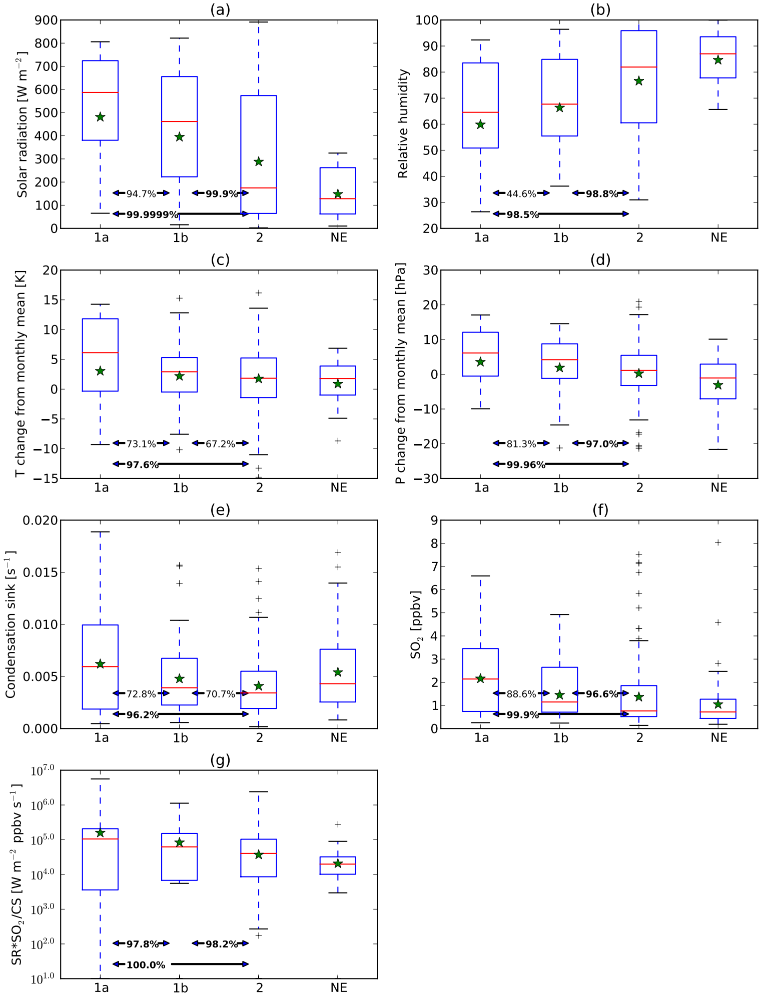

ACPD
14, 707–750, 2014

New-particle formation, growth and climate-relevant particle production

J. R. Pierce et al.

Title Page
Abstract | Introduction
Conclusions | References
Tables | Figures
◀◀ | ▶▶
◀ | ▶
Back | Close
Full Screen / Esc
Printer-friendly Version
Interactive Discussion

Fig. 4. Box-whisker plots of various meteorological variables as well as the condensation sink, SO_2 mixing ratio and a H_2SO_4 proxy for class 1a, 1b, 2 and non-event days. The values are calculated between the start and end of new-particle formation on each day except for non-event days where the full day is used. The red line shows the median values. Stars show the mean values. The box shows the interquartile range (IQR, 25th and 75th percentile). The whiskers show the lowest datum still within 1.5 IQR of the lower quartile, and the highest datum still within 1.5 IQR of the upper quartile. Crosses show data outside of 1.5 IQR above or below the upper or lower quartile. The percentages shown in between each box show the probability that the distributions are statistically different (calculated using the Mann–Whitney U test). Although not shown on the plots, the distributions for 1a days are statistically different from non-event days to at least the 98 % level for all factors except condensation sink (89 %). Panel **(a)** solar radiation, **(b)** relative humidity, **(c)** temperature change from the running 28 day mean (14 days before to 14 days after, to remove the season cycle), **(d)** surface pressure change from the running 28 day mean, **(e)** condensation sink, **(f)** SO_2 mixing ratio, **(g)** H_2SO_4 proxy ($SR \cdot SO_2$/condensation_sink).

ACPD
14, 707–750, 2014

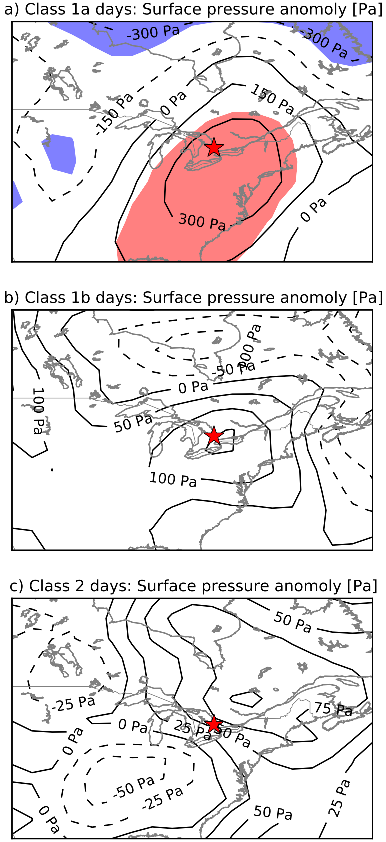

Fig. 5. NCEP reanalysis surface pressure anomaly [Pa] from the 28 day mean for **(a)** class 1a days, **(b)** 1b days, **(c)** 2 days. Positive 95 % significance anomalies are shaded in pink and negative 95 % significance anomalies are shaded in blue.

ACPD
14, 707–750, 2014

New-particle formation, growth and climate-relevant particle production

J. R. Pierce et al.

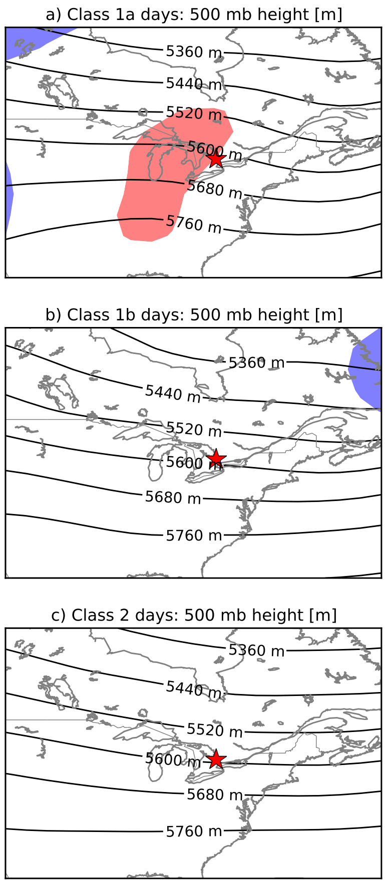

Fig. 6. NCEP reanalysis mean 500 mb geopotential heights [m] for **(a)** class 1a days, **(b)** 1b days, **(c)** 2 days. Positive 95 % significance anomalies are shaded in pink and negative 95 % significance anomalies are shaded in blue.

ACPD
14, 707–750, 2014

New-particle formation, growth and climate-relevant particle production

J. R. Pierce et al.

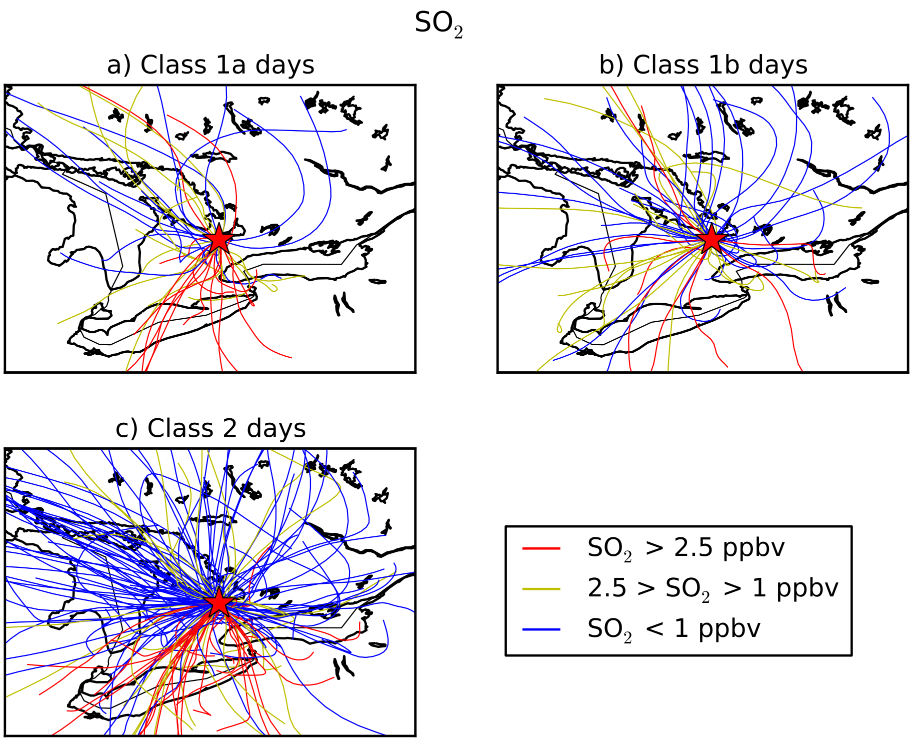

Fig. 7. 24 h back trajectories arriving during the new-particle formation event during each class 1a, 1b and 2 day (one back trajectory per event). Trajectories are color-coded by the SO_2 concentration measured during the event.

ACPD
14, 707–750, 2014

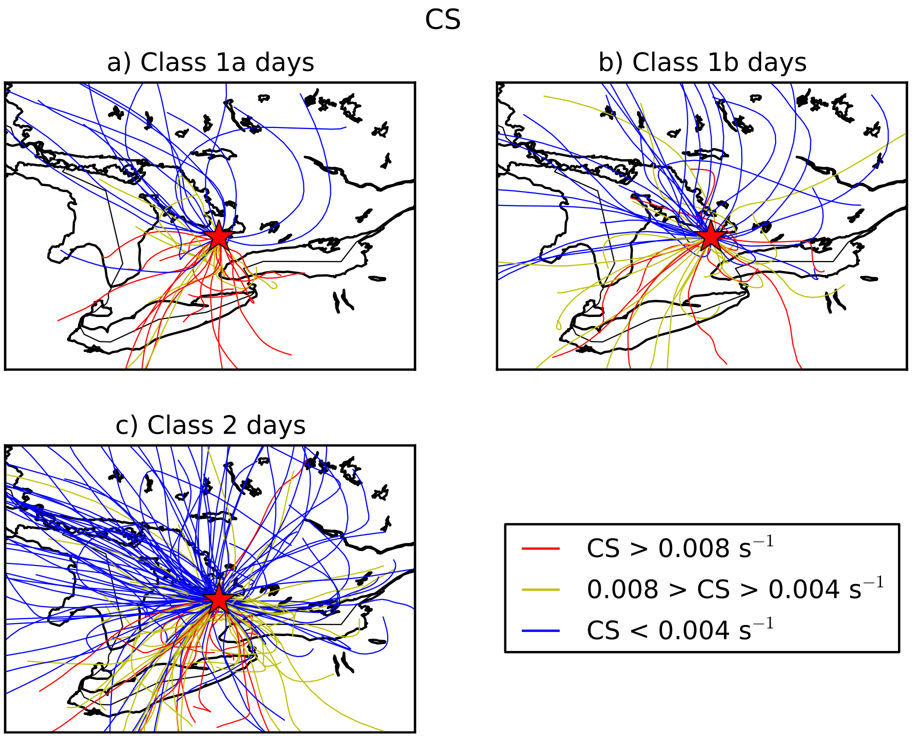

Fig. 8. 24 h back trajectories arriving during the new-particle formation event during each class 1a, 1b and 2 day (one back trajectory per event). Trajectories are color-coded by the condensation sink measured during the event.

ACPD
14, 707–750, 2014

New-particle formation, growth and climate-relevant particle production

J. R. Pierce et al.

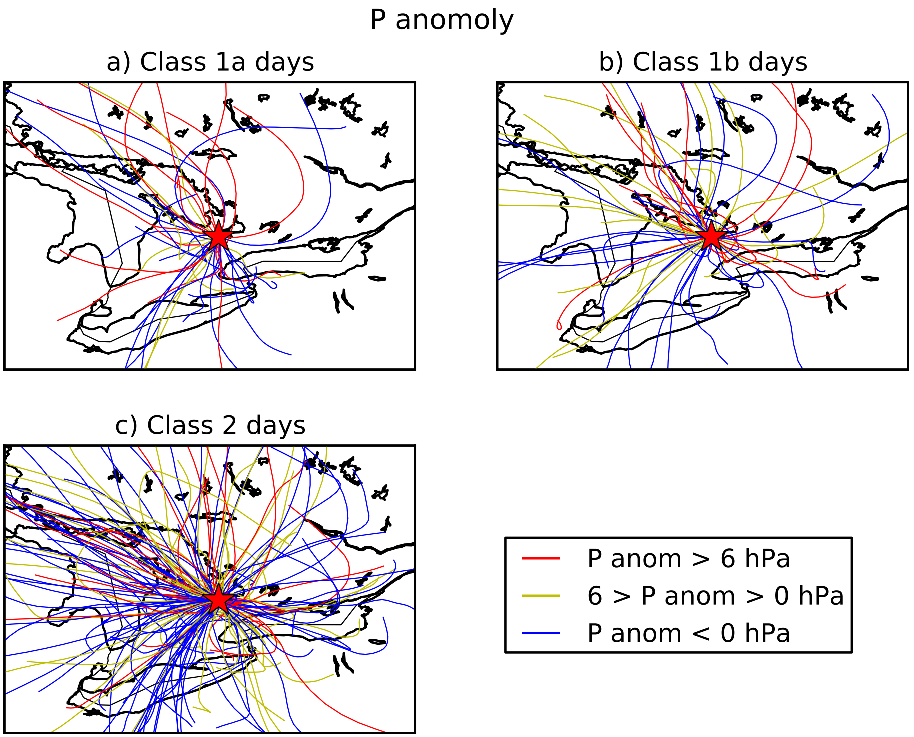

Fig. 9. 24 h back trajectories arriving during the new-particle formation event during each class 1a, 1b and 2 day (one back trajectory per event). Trajectories are color-coded by the surface pressure anomaly (from the 28 day running mean) measured during the event.

ACPD
14, 707–750, 2014

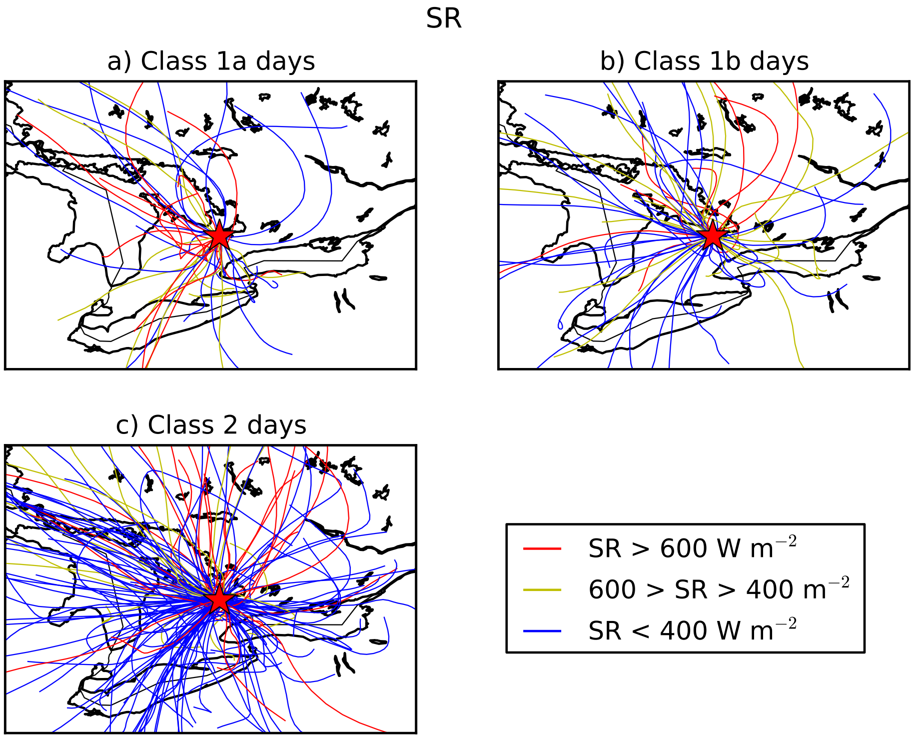

Fig. 10. 24 h back trajectories arriving during the new-particle formation event during each class 1a, 1b and 2 day (one back trajectory per event). Trajectories are color-coded by the solar radiation measured during the event.

ACPD
14, 707–750, 2014

New-particle formation, growth and climate-relevant particle production

J. R. Pierce et al.